coatings

MDPI

Article

Strong Coupling between Tamm and Surface Plasmons for Advanced Optical Bio-Sensing

Zigmas Balevičius

Faculty of Electronics, Vilnius Gediminas Technical University, Naugarduko St. 41, 03227 Vilnius, Lithuania; zigmas.balevicius@vgtu.lt; Tel.: +37-068579015

Received: 12 November 2020; Accepted: 3 December 2020; Published: 5 December 2020

Abstract: The total internal reflection ellipsometry method was used to analyse the angular spectra of the hybrid Tamm and surface plasmon modes and to compare their results with those obtained using the conventional single SPR method. As such type of measurement is quite common in commercial SPR devices, more detailed attention was paid to the analysis of the p-polarization reflection intensity dependence. The conducted study showed that the presence of strong coupling in the hybrid plasmonic modes increases the sensitivity of the plasmonic-based sensors due to the reduced losses in the metal layer. The experimental results and analysis of the optical responses of three different plasmonic-based samples indicated that the optimized Tamm plasmons $\Delta R_{p(TP)}$ and optimized surface plasmons $\Delta R_{p(SP)}$ samples produce a response that is about five and six times greater than the conventional surface plasmon resonance $\Delta R_{p(SPR)}$ in angular spectra. The sensitivity of the refractive index unit of the spectroscopic measurements for the optimized Tamm plasmon samples was 1.5 times higher than for conventional SPR, while for wavelength scanning, the SPR overcame the optimized TP by 1.5 times.

Keywords: strong coupling; Tamm plasmons; surface plasmons; hybrid plasmonic modes; optical biosensors

1. Introduction

Sensors based on optical signal interrogation are widely used for the detection of biochemical interactions at solid–liquid interfaces, for the monitoring of various chemicals adsorbed on surfaces [1,2] and for the evaluation of the refractive indexes of liquids [3]. For this purpose, surface plasmon resonance (SPR) optical sensors are most widely used [4,5]. Surface plasmon polariton (SPP) based optical sensors are able to detect the kinetics of various biochemical interactions such as antibody–antigen binding [4] and to determine, for instance, the adsorbed surface mass in monolayers of proteins [5]. The non-destructive, label-free, high sensitivity and real time monitoring ability of this optical signal makes this plasmonic based sensing technique an extremely attractive tool for the analysis of a wide range of surface science areas [6]. The high sensitivity of the optical signal registration is achieved due to the strong localization of the electric field at the metal/dielectric interface when resonance conditions for such light–matter interaction are satisfied [7]. The SPP is a non-radiative electromagnetic waves, which can be excited by light through a glass prism or grating coupler which are necessary to match the in-plane wave vectors of the incident light and the plasmons in the metal layer. This rather strong light–matter interaction leads the properties of the dispersion relation (angular frequency (ω) and in-plane wavevector (k)) of the surface plasmon polaritons which are sensitive to the any perturbation of the refractive index changes on the SPP supported interfaces. However, the rather broad width of such SPP resonances, caused by the large absorption and scattering losses in the metal layer, limits the further improvement of the sensitivity of this type of optical sensor. These losses in the metals are determined by the imaginary part of their relative permittivity [8]. They shorten the

propagation length of the SPP waves and increase the width of the resonance. Thus, the appropriate dielectric function of the metal layer optimized for high sensitivity requires a larger negative real part and a smaller imaginary part of this dielectric function.

This fundamental property of metals limits the further development not only of this sensing application [9], but also of similar developments in fields such as integrated photonic components, optical filters, lasing, and others [10]. Bloch surface waves (BSWs) can be generated at the surfaces of photonic crystals (PCs) and dielectrics [11]. As for the SPR, a coupler (glass prism or grating) is required for the excitation of such BSWs in order to satisfy the matching conditions of the in-plane wave vectors in the stop band of the photonic crystal [3,10]. The use, however, of only dielectric materials significantly narrows the width of these resonances as the dielectric function of such dielectric materials are weakly dispersive compared to metals. Due to weak dispersion of BSW the sensitivity to the refractive index changes are lower than for SPR. Advantages in sensitivity, however, are achievable due to the steeper slope of the Bloch surface wave resonances.

Between the SPP and BSW, the intermediate type of electromagnetic surface waves which exist between the metal and photonic crystals are the so-called Tamm plasmon polaritons (TPP) [12]. These types of optical states are similar to the electron states proposed by I. Tamm [13]. In the case of photonic crystals, the Bragg reflections form a photonic stop band for the photons, which act as the energy band gap of the real crystals. The TPPs share the optical properties of both the SPP and the BSW. The resonant oscillations of the free electrons in the metal, like for the SPPs, are involved in the TP excitation and are non-propagating states which can be excited in both the TM and TE polarizations, like the Bloch surface waves on the interfaces between the PC and the dielectric [14]. Another important feature of the TPPs are that they have an in-plane wave vector which is less than the wave vector of light in a vacuum. Thus, a direct optical excitation of these TPPs is possible, contrary to the SPPs, where the light wave vector is always smaller than the SPP. In cases where the conditions for these excitations are satisfied for both the resonances of the SPPs and TPPs, a hybrid plasmonic mode appears [15]. Such situations can be realized whenever a glass prism is optically connected to a PC on which a thin metal layer is deposited. In such systems, the TPP and SPP resonances exist in a broad range of angles of light incident (AOI) to the prism. At certain AOIs to the prism corresponding to the same wavevectors at which both the SPPs and TPPs can be excited, the reflectance spectrum is changed, and the dispersion relations of both excitations are modified. In most cases, these changes in the reflectance and dispersion relations indicate a strong coupling regime between the TPPs and SPPs.

Recently much attention has been paid to the study of strong coupling between these plasmon active metal nanostructures and the various emitters such as excitons in semiconductors, in dyes or in photochromic molecules [16–18]. The main feature of this strong coupling regime is that the energy exchange between the plasmons and the emitters occurs during a coherent time [19]. This means that in such coupled systems, the coupling strength between the plasmons and the emitters exceeds the damping rate and as a result, hybrid modes are created [20]. These hybrid modes can be achieved when the interactions are sufficiently strong, and the energy spectrum is modified, compared to the spectral positions of single resonances in non-coupled systems. In fact, these hybrid modes are polaritons formed partially from plasmons and emitters [21]. However, the existence of hybrid Tamm and surface plasmon modes were also demonstrated [15]. The presence of strong coupling between the TPP and the SPP lead to the anti-crossing of their dispersion curves and, as a result, narrow the width of their resonances. It has been shown that in its optimized hybrid TPP-SPP mode, the dispersion of the SPP branch can have reduced losses [22]. The splitting gap between the TPP and the SPP components in this new hybrid mode corresponds to their coupling strength [23]. The changes in the gap between the TPP and the SPP reflectance minimums and the widening or narrowing of the resonances indicate variations of their coupling strength.

The excitation of these hybrid TPP–SPP plasmonic modes require conditions of total internal reflection. These states are also polarization sensitive. Detailed analysis of the polarization properties in such TIR setups can be achieved by using total internal reflection ellipsometry (TIRE) [24]. TIRE is a technique combining spectroscopic ellipsometry and the analysis of surface plasmon electromagnetic waves. The sensitivity of this method is higher compared to that of conventional ellipsometry or SPR [25,26]. In fact, TIRE utilizes the analytical power of ellipsometry and increases its sensitivity by introducing the SPR effect into the operation scheme of the ellipsometer.

Studies employing the strong coupling effect between the TPP and SPP in the spectroscopic mode have been performed before, where changes in the resonant wavelength were registered [22]. However, most commercially available plasmonic sensors use the p-polarized intensity at fixed wavelengths and scanning angles of incidence. This study demonstrates that increased sensitivity to the p-polarization reflection due to the narrowing of the resonance width caused by strong coupling between TPP and SPP can be achieved not only for the wavelength, but also for the angle of incidence scanning.

2. Materials and Methods

Three samples were investigated. These consisted of two structures supporting optimized hybrid Tamm-surface plasmons modes and a commercially available Xantec surface plasmon resonance (SPR) chip. The first two slightly different photonic structures of hybrid plasmonic modes were optimized for enhanced sensitivity of these particular excitation components (Tamm plasmons or surface plasmons). For the optimized surface plasmon (SP) components in their hybrid modes, distributed Bragg gratings consisting of 6 bilayers of ~120 nm TiO_2/~200 nm SiO_2 and a 30 nm TiO_2 layer on top were formed on BK7 glass substrates. For the optimized Tamm plasmon component, the distributed Bragg grating consisted of five bilayers of ~120 nm TiO_2/~200 nm SiO_2 formed on a BK7 glass substrate. These Bragg gratings were created by ion beam sputtering. Afterwards, thin gold (~40 nm) layers were deposited on both photonic crystal structures by magnetron sputtering. The SPR sample consisted of a gold film having a thickness of about 45 nm and about 2 nm underlayer of Ti for better adhesion.

The total internal reflection ellipsometry (TIRE) experiments were then conducted using a dual rotating compensator ellipsometer RC2 (J.A. Woollam Co., Inc., Lincoln, NE, USA). The spectroscopic ellipsometry experiments were carried out in the 400–1000 nm spectral range. For all the samples with the supported hybrid plasmonic modes and the SPR, the experiments were conducted in a TIRE configuration. These used a half-cylindrical BK7 glass prism in the range of angle of incidence (AOI) 60°–75° connected via a refractive index matching fluid with investigated samples (Figure 1). To compensate for the light beam focusing effect due to the semi-cylindrical prism, lenses with a 40 mm focal length were used for the pre-focusing of the incoming and reflected light to the detector.

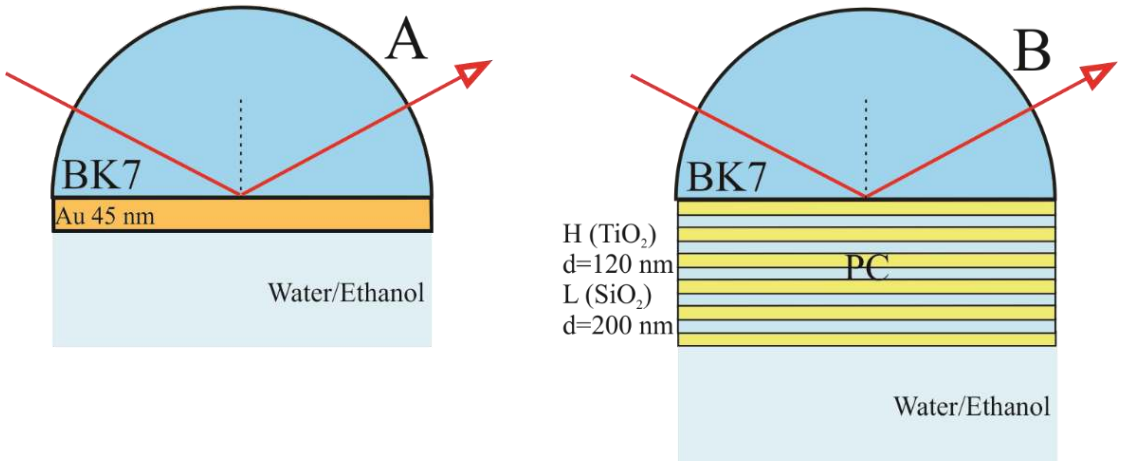

Figure 1. *Cont.*

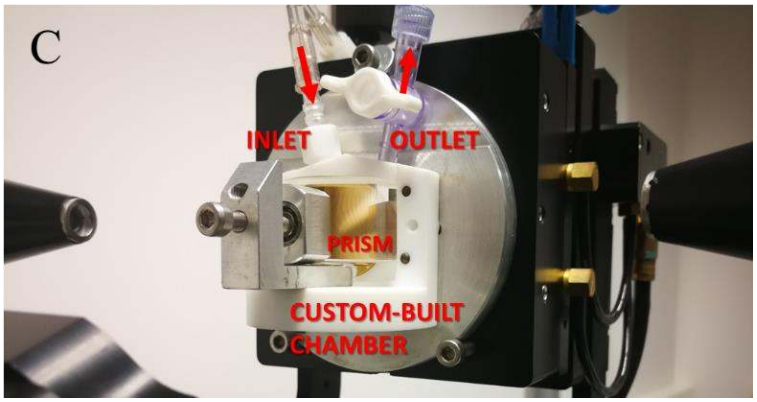

Figure 1. Samples structures and measurements configurations for single SPR (**A**) and for optimized Tamm plasmons and optimized surface plasmons samples (**B**) and the custom-built chamber connected with glass prism and sensor chip (**C**).

A liquid handling system with a custom-built Teflon chamber was used in which the surfaces of all the samples were placed. This chamber was filled with deionized water, which was then changed to deionized water/ethanol (50%/50%) mixture, whose refractive index is higher than that of pure deionized water. The measured experimental data of the ellipsometric parameters Ψ(λ) and Δ(λ) were then expressed as the p-polarized intensity, using the data acquisition software CompleteEase (J.A. Woollam Co., Inc.), and were then presented as the p-intensity map dependence on the wavelength (λ) vs. angle of incidence (θ°) (Figures 2 and 3). These p-polarized intensity maps, in fact, represent the dispersion relations of the investigated plasmonic excitations. Furthermore, a fixed resonant wavelengths λ = 800 nm (SP), λ = 715 nm (TP), and λ = 820 nm (Hybrid TP-SP) were chosen to demonstrate the optimized sensitivity properties in the angular spectra of the p-intensity polarizations for SPR and Tamm plasmon polaritons and hybrid TPP-SPP mode (Figure 4).

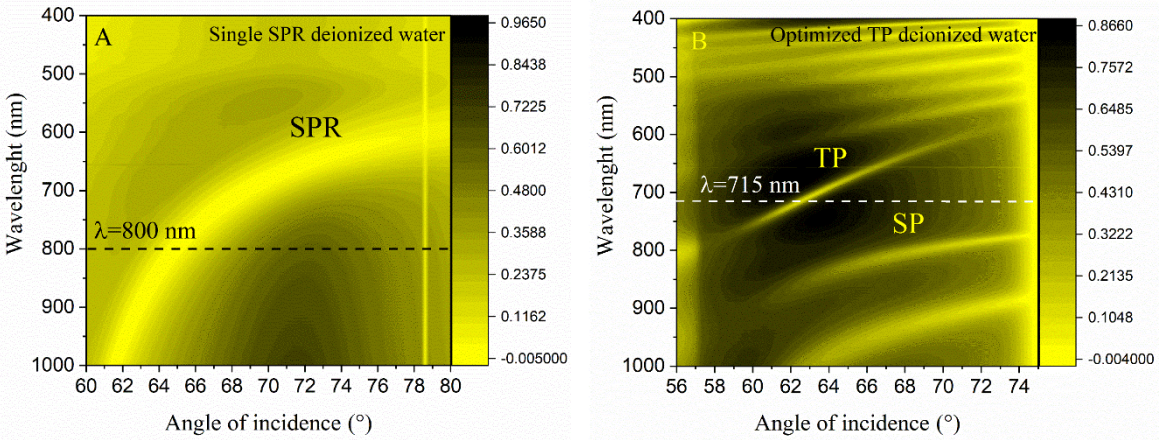

Figure 2. *Cont.*

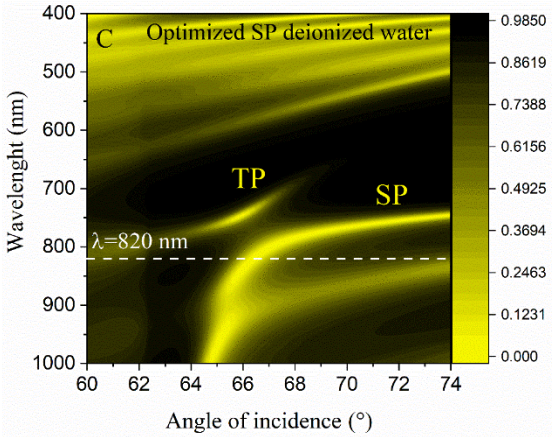

Figure 2. Experimentally measured p-intensity dispersion relations in deionized water solution of the single SPR mode in a Cr/Au (50 nm) structure (**A**), the optimized Tamm plasmon mode (**B**) generated in the photonic structure of five bilayers (TiO_2/SiO_2 (120 nm/200 nm))/Au (40 nm) and optimized surface plasmon mode (SP) in hybrid plasmonic mode consisted from six bilayers (TiO_2/SiO_2 (120 nm/200 nm))/40 nm TiO_2/Au (40 nm) (**C**). The white dashed lines indicate the cross-section at fixed wavelength which were chosen to present the angular dependence of plasmonic excitations on the p-polarized intensity.

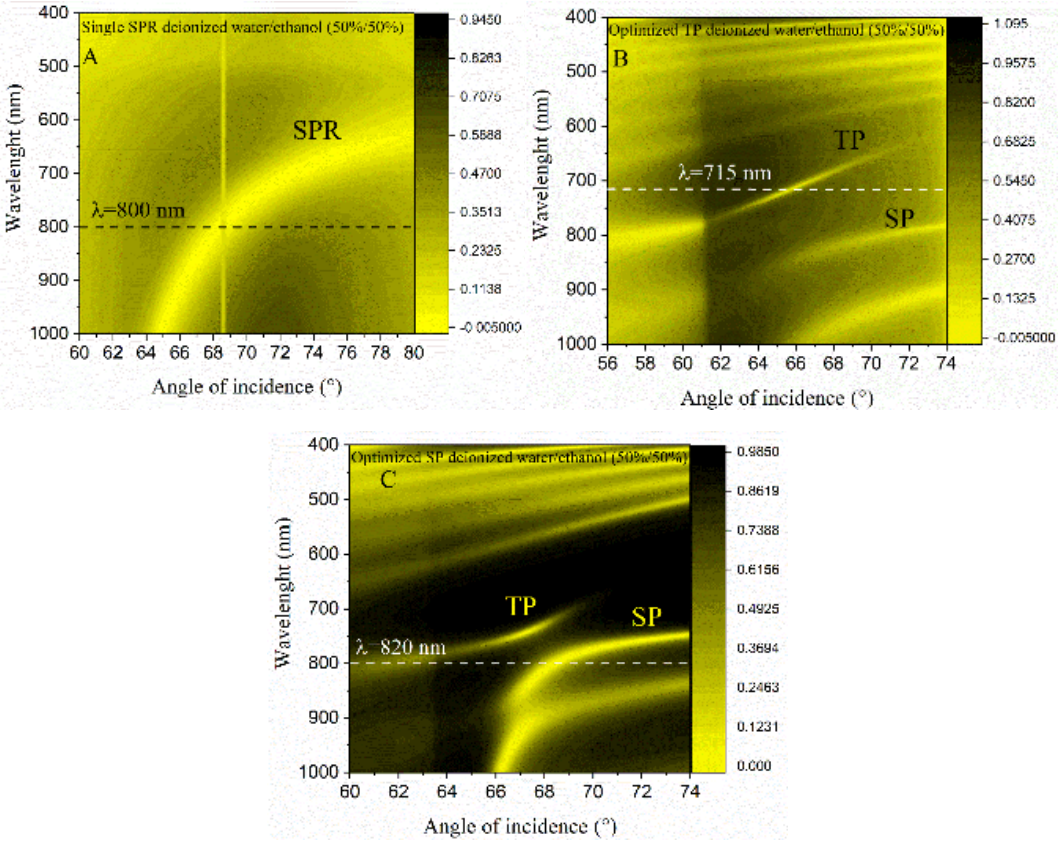

Figure 3. Experimentally measured p-intensity dispersion relations in deionized water/ethanol (50%/50%) mixed solution of the single SPR mode in a Cr/Au (50 nm) structure (**A**), the optimized Tamm plasmon mode (TP) (**B**) generated in the photonic structure of five bilayers (TiO_2/SiO_2 (120 nm/200 nm))/Au (40 nm) and optimized surface plasmon mode (SP) in hybrid plasmonic mode consisted from six bilayers (TiO_2/SiO_2 (120 nm/200 nm))/40 nm TiO_2/Au (40 nm) (**C**). The white dashed lines indicate the cross-section at fixed wavelength which were chosen to present the angular dependence of plasmonic excitations on the p-polarized intensity.

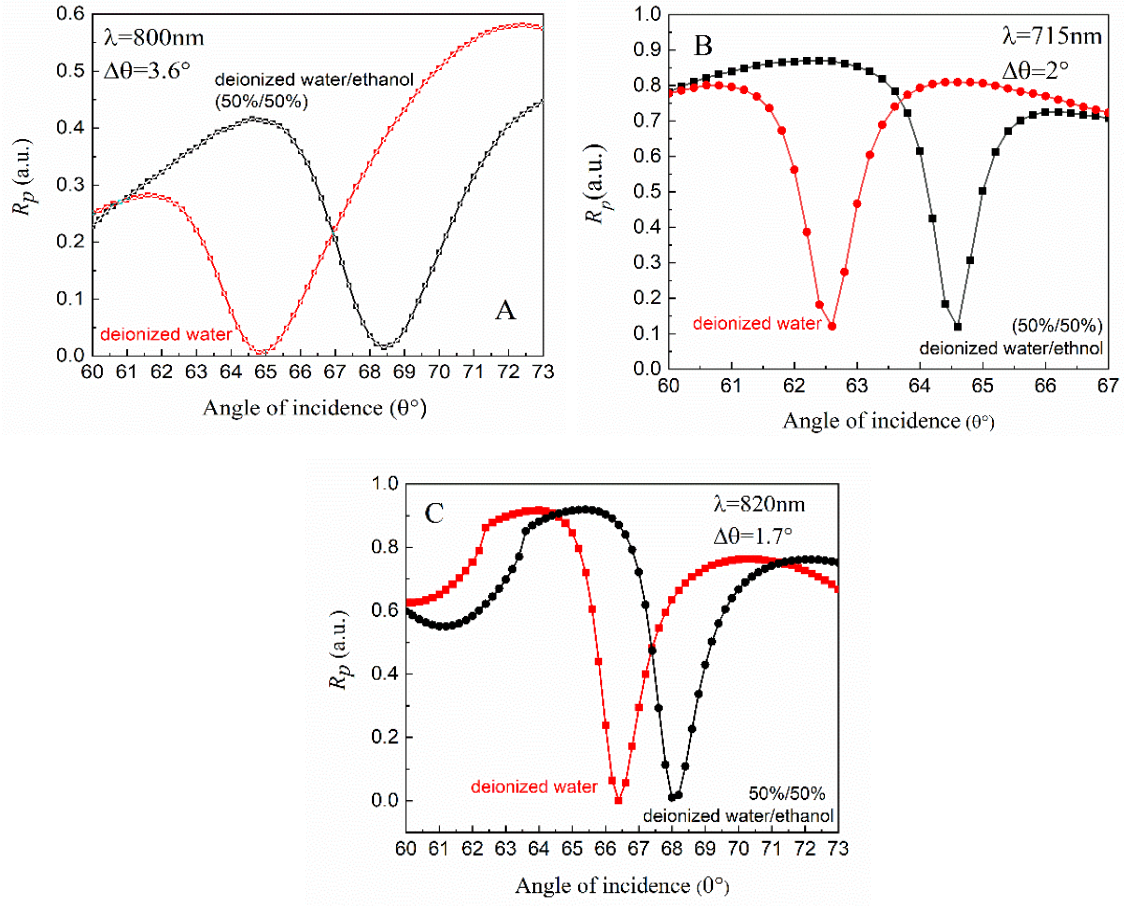

Figure 4. Experimental spectra of p-intensity dependence on the AOI for single SPR (**A**), optimized Tamm plasmon (TP) (**B**), and optimized surface plasmon (SP) (**C**) samples before (red curves) and after (black curves) deionized water changed to solution of deionized water/ethanol (50%/50%). The spectra corresponds to the cross-sections in the Figures 3 and 4.

3. Results and Discussions

It has been shown before that by applying spectroscopic ellipsometry in its total internal reflection configuration and the so-called total internal reflection ellipsometry (TIRE), a higher sensitivity to the refractive index and the attached surface mass can be achieved compared with that produced by standard commercially available surface plasmon resonance biosensors [27]. This improved sensitivity was obtained mainly due to the ability to directly measure the phase difference between s- and p-polarized reflected waves in the vicinity of the SPR, where the phases of the reflected waves change drastically [25]. Moreover, TIRE has a better sensitivity to even the ellipsometric parameter Ψ than the standard p-polarized intensity measurement which is obtained by the SPR [24]. The TIRE with a hybrid plasmonic mode of Tamm and surface plasmons were applied for saturated gas [28], graphene influence to the strong coupling [29] and biosensing [22], where the strong coupling effect between these two excitations was employed. However, commercially available SPR biosensors normally use simpler optical schemes, where only the p-polarized intensity of the SPR phenomenon is registered and which use only a single wavelength as the light source. In this study, the TIRE method was used for the analysis of the optical properties and sensitivity features of the Tamm-surface plasmon hybrid modes. Their p-polarized intensity for a single wavelength and the p-polarized signal intensity of the hybrid Tamm-surface plasmon mode were then compared with the single SPR used in standard optical biosensors. As mentioned before, three samples were used: the single thin gold layer for the SPR and the two photonic crystals (PC)/Au structures with optimized sensitivity for Tamm plasmons and for surface plasmons in their hybrid plasmonic modes, respectively.

In order to determine the wavelength at which the resonant effect of the plasmonic excitation was most efficient, the dispersion relations for all three samples were first measured experimentally and presented as maps of the p-polarized intensity of wavelength dependence on the angle of incidence (AOI). Figure 2A represents the single SPR excitation and Figure 2B,C, the hybrid Tamm-surface plasmon modes for slightly different multi-layered structures. As can be seen, the dispersion relation of the single SPR lies in the 650–700 nm spectral range for angles of incidence 70–75°, while for the hybrid plasmonic modes, the SPP branch moves down to the longer wavelengths and lies at about 800 nm for the same AOI. Such modification of dispersion relation for SPP branch caused by strong coupling between Tamm optical states and surface plasmon polariton in the hybrid plasmonic mode.

Such behavior is the result of the strong coupling effect between the Tamm plasmons and the surface plasmons, together with a narrowing of the excitation line of the SP branch in this AOI range, compared with that of a single SPR. The narrowing of the dispersion relation line indicates the lower losses of such SP in its hybrid mode. Attention should also be paid to the Tamm plasmon branch in its hybrid plasmonic mode which lies between 600–800 nm in a wide range angle of incidence and has an even narrower width than the SP branch. The cross-section at the resonant wavelength is marked with dashed lines in each spectra of the dispersion relation. In Figure 2, the presented dispersion relations correspond to the optical responses to the ambient medium of deionized water, while in Figure 3, the dispersion relations for all three samples are presented when responding to a mixture of deionized water (50%) and ethanol (50%) which changes the refractive index of the ambient medium. The cross-sections (dash lines) were made at the same resonant wavelength as with the pure deionized water.

The cross-sections at a particular resonant wavelength give the angular spectra of the p-polarized intensity of the corresponding excitations (Figure 4A–C). The black curves correspond to the optical responses in the vicinity of the plasmonic excitations for deionized water and the red curves show the changes in the optical response of the system when the refractive index changes due to the mixture of deionized water (50%) and ethanol (50%). As can be seen from Figure 4B, the sample optimized for the Tamm plasmons manifested itself at the AOI = 62.5° and $\lambda_{TP} = 715$ nm for the deionized water and AOI = 64.5° for the mixture of water/ethanol (50%/50%), respectively. This corresponded to a shift of 2° degrees for the refractive index change $\delta n_{(\lambda=715\ \mathrm{nm})} = 1.3442 - 1.3298 = 0.0144$. It should be noted that the full width at half maximum (FWHM) for the Tamm plasmon excitation in the hybrid mode was 0.88°. In the case of the multilayer sample for optimized surface plasmons in their hybrid plasmonic modes, the angular shift was 1.7°, i.e., from 66.4° up to 68.1° (Figure 4C) and the FWHM = 1.56° to $\lambda_{SP} = 820$ nm, $\delta n_{(\lambda=820\ \mathrm{nm})} = 1.3425 - 1.32979 = 0.0146$. The same measurements were performed with the commercially available SPR chip consisted of a thin (~45 nm) gold layer without any additional multi-layered structures. The SPR shift to the larger AOI due to changes of the refractive index of the ambient (liquid) was 3.5°, i.e., from 64.9° up to 68.5° (Figure 4A) and the FWHM = 3.5° for the $\lambda_{SPR} = 800$ nm, $\delta n_{(\lambda=800\ \mathrm{nm})} = 1.3428 - 1.3282 = 0.016$. However, a much wider FWHM was registered for the SPR. This was 3.6°, which indicated significantly higher metal losses for these plasmonic excitations compared with the Tamm plasmons or the surface plasmons in their hybrid plasmonic modes. The narrowing of the width of the hybrid plasmonic resonances due to such reduced losses leads to the increased values of the p-intensity reflectance for the TP $\delta R_{TP} \approx 0.75$ and SP $\delta R_{TP} \approx 0.87$ compared with the single SPR, which indicated that this was $\delta R_{TP} \approx 0.16$. As a result, these numbers led to a corresponding sensitivity of the refractive index unit of $\frac{\Delta R_{p(TP)}}{\delta n} = \frac{0.75}{0.0144} = 52\ RIU^{-1}$, $\frac{\Delta R_{p(SP)}}{\delta n} = \frac{0.87}{0.0146} = 60\ RIU^{-1}$ and $\frac{\Delta R_{p(SPR)}}{\delta n} = \frac{0.16}{0.016} = 10\ RIU^{-1}$. The experimental results and analysis of the optical responses of these three different plasmonic based samples showed that the optimized Tamm plasmons $\Delta R_{p(TP)}$ and optimized surface plasmons $\Delta R_{p(SP)}$ samples produced five and six times better responses than the conventional surface plasmon resonance $\Delta R_{p(SPR)}$. Meanwhile, the conventional SPR overcame the optimized hybrid plasmonic modes for the registration of changes of the angle of incidence. These were by TP = 1.75 and SP = 2 times, respectively.

As variable angle spectroscopic ellipsometry gives the possibility of analysing the optical response by using a full analysis of the polarized light, the p-polarized intensity spectra dependence on the wavelength was also presented (Figure 5A,B). It should be noted that focusing on only the p-polarized light is related to the studied plasmonic excitations, which are generated only in this state of light polarisation. As was noted above [22], the surface plasmon polariton component in its hybrid plasmonic mode produces a higher sensitivity than was achievable when using the single SPR for the bovine serum albumin protein covalent immobilization.

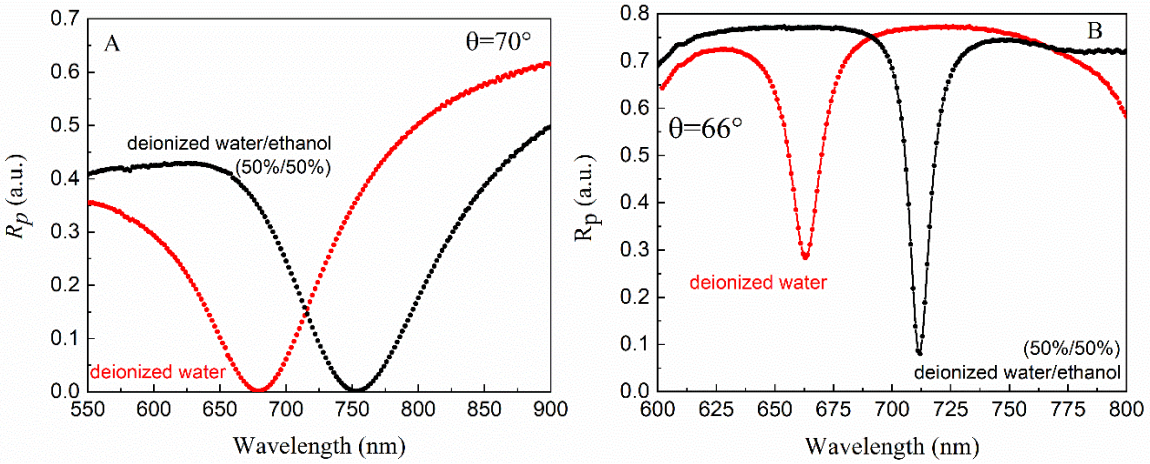

Figure 5. Experimental spectra of p-intensity dependence on the wavelength for single SPR (**A**) and optimized Tamm plasmon (TP) (**B**) samples before (red curves) and after (black curves) deionized water changed to solution of deionized water/ethanol (50%/50%).

Thus, this study was focused on achieving a higher sensitivity for the Tamm plasmon component in its hybrid plasmonic mode. The AOI was optimized for the TP and the conventional SPR samples were chosen so that the highest sensitivity would be achieved for both. The single SPR of the commercially available chip manifested itself as producing a dip in the p-polarized intensity spectra at 680 nm and AOI = 70°. After changing the deionized water with a mixture of water/ethanol (50%/50%), the resonance dip red shifted up to 754 nm (Figure 5A). For the Tamm plasmon optimized structure, the plasmonic dip was at the 663 nm for AOI = 66° and after increasing the refractive index of liquid, the dip moved to a longer wavelength, i.e., up to 712 nm (Figure 5B). After changing the deionized water with the water/ethanol mixture, the increased refractive index of the liquid shifted in both plasmonic excitations to longer wavelengths. For the single SPR, the red shift was 72 nm and this corresponded to the p-intensity changes in $\delta R_p = 0.36$. For the Tamm plasmon optimized sample, the spectral changes were smaller ~50 nm. However, such a red shift induced a change in the relative p-intensity of about $\delta R_p \approx 0.54$. For both resonances, the differences in the refractive index of the liquid was the same $\delta n = 0.015$. Thus, as can be seen from Figure 5B, the red shift of the Tamm plasmon component was significant and the δR_p value was evaluated from the simulation of the red shift with the smaller changes of the refractive index of liquid, but taking into account the experimental red shift as a reference. The evaluated sensitivity to the refractive indexes were $\frac{\Delta R_{p(TP)}}{\delta n} = \frac{0.54}{0.015} = 36\ RIU^{-1}$ and $\frac{\Delta R_{p(SPR)}}{\delta n} = \frac{0.36}{0.015} = 24\ RIU^{-1}$, respectively. Meanwhile, the spectral shift of these resonances gave the corresponding sensitivities $\frac{\Delta\lambda_{(TP)}}{\delta n} = \frac{50}{0.015} = 3266\ \mathrm{nm}/RIU$ and $\frac{\Delta\lambda_{(SPR)}}{\delta n} = \frac{74}{0.015} = 4933\ \mathrm{nm}/RIU$. These evaluations led to the following estimations of the sensitivity of the hybrid plasmonic modes and the conventional SPR to the RIU. For the optimized Tamm plasmon sample, the p-intensity measurement was 1.5 times higher than for the conventional SPR. For the wavelength scanning, however, the SPR overcame the optimized TP by 1.5 times.

4. Conclusions

Summarizing, the TIRE method was used for the analysis of the angular spectra of the hybrid Tamm and surface plasmon modes and their comparison with those produced by conventional single SPRs. A more detailed analysis was made of the p-reflection intensity dependence on the AOI because such types of measurements are very common in commercial SPR devices. The conducted study showed that the presence of strong coupling in the hybrid plasmonic modes increases the p-polarized intensity sensitivity of such excitations due to the reduced losses in the metal layers. It should be noted that conventional SPR shows better sensitivity for AOI and wavelength scanning, while the registration of p-intensity changes gives better values for the optimized plasmonic modes. The angular spectra of the hybrid plasmonic modes with the strong coupling effect was analyzed for the first time in our knowledge. The strong coupling effect in the hybrid plasmonic modes allow one to control and tune the dispersion relation of the plasmonic excitations for corresponding purposes. Since modern coating technologies allow the production of nanometric structures with high precision, this produces the possibility of designing nanophotonic devices with advanced properties.

Funding: This research received no external funding.

Acknowledgments: The authors thank for technical support in the photonic crystals preparation T. Tolenis and A. Valavičius.

Conflicts of Interest: The author declares no conflict of interest.

References

1. Hu, J.; Ma, L.; Wang, S.; Yang, J.; Chang, K.; Hu, X.; Sun, X.; Chen, R.; Jiang, M.; Zhu, J.; et al. Biomolecular interaction analysis using an optical surface plasmon resonance biosensor: The marquardt algorithm vs newton iteration algorithm. *PLoS ONE* **2015**, *10*, e0132098. [CrossRef] [PubMed]
2. Liedberg, B.; Nylander, C.; Lundström, I. Biosensing with surface plasmon resonance—How it all started. *Biosens. Bioelectron.* **1995**, *10*, i–ix. [CrossRef]
3. Balevicius, Z.; Baskys, A. Optical dispersions of bloch surface waves and surface plasmon polaritons: Towards advanced biosensors. *Materials* **2019**, *12*, 3147. [CrossRef] [PubMed]
4. Kravets, V.G.; Schedin, F.; Jalil, R.; Britnell, L.; Gorbachev, R.V.; Ansell, D.; Thackray, B.; Novoselov, K.S.; Geim, A.K.; Kabashin, A.V.; et al. Singular phase nano-optics in plasmonic metamaterials for label-free single-molecule detection. *Nat. Mater.* **2013**, *12*, 304–309. [CrossRef] [PubMed]
5. Wang, W.; Yang, Y.; Wang, S.; Nagaraj, V.J.; Liu, Q.; Wu, J.; Tao, N. Label-free measuring and mapping of binding kinetics of membrane proteins in single living cells. *Nat. Chem.* **2012**, *4*, 846–853. [CrossRef]
6. Zhou, J.; Qi, Q.; Wang, C.; Qian, Y.; Liu, G.; Wang, Y.; Fu, L. Surface plasmon resonance (SPR) biosensors for food allergen detection in food matrices. *Biosens. Bioelectron.* **2019**, *142*, 111449. [CrossRef]
7. Barnes, W.L. Surface plasmon–polariton length scales: A route to sub-wavelength optics. *J. Opt. A Pure Appl. Opt.* **2006**, *8*, S87–S93. [CrossRef]
8. Raether, H. Surface plasmons on smooth surfaces. In *Surface Plasmons on Smooth and Rough Surfaces and on Gratings*; Springer Tracts in Modern Physics; Springer: Berlin/Heidelberg, Germany, 1988; Volume 111, pp. 4–39, ISBN 978-3-540-17363-2.
9. Sinibaldi, A.; Danz, N.; Descrovi, E.; Munzert, P.; Schulz, U.; Sonntag, F.; Dominici, L.; Michelotti, F. Direct comparison of the performance of Bloch surface wave and surface plasmon polariton sensors. *Sens. Actuators B Chem.* **2012**, *174*, 292–298. [CrossRef]
10. Kovalevich, T.; Ndao, A.; Suarez, M.; Tumenas, S.; Balevicius, Z.; Ramanavicius, A.; Baleviciute, I.; Häyrinen, M.; Roussey, M.; Kuittinen, M.; et al. Tunable Bloch surface waves in anisotropic photonic crystals based on lithium niobate thin films. *Opt. Lett.* **2016**, *41*, 5616. [CrossRef]
11. Yeh, P.; Yariv, A.; Hong, C.-S. Electromagnetic propagation in periodic stratified media. I. General theory. *J. Opt. Soc. Am.* **1977**, *67*, 423. [CrossRef]
12. Sasin, M.E.; Seisyan, R.P.; Kaliteevski, M.A.; Brand, S.; Abram, R.A.; Chamberlain, J.M.; Iorsh, I.V.; Shelykh, I.A.; Egorov, A.Y.; Vasil'ev, A.P.; et al. Tamm plasmon-polaritons: First experimental observation. *Superlattices Microstruct.* **2010**, *47*, 44–49. [CrossRef]

13. Tamm, I. Über eine mögliche art der elektronenbindung an kristalloberflächen. *Z. Phys.* **1932**, *76*, 849–850. [CrossRef]
14. Kaliteevski, M.; Iorsh, I.; Brand, S.; Abram, R.A.; Chamberlain, J.M.; Kavokin, A.V.; Shelykh, I.A. Tamm plasmon-polaritons: Possible electromagnetic states at the interface of a metal and a dielectric Bragg mirror. *Phys. Rev. B* **2007**, *76*, 165415. [CrossRef]
15. Afinogenov, B.I.; Bessonov, V.O.; Nikulin, A.A.; Fedyanin, A.A. Observation of hybrid state of Tamm and surface plasmon-polaritons in one-dimensional photonic crystals. *Appl. Phys. Lett.* **2013**, *103*, 061112. [CrossRef]
16. Andrew, P. Energy transfer across a metal film mediated by surface plasmon polaritons. *Science* **2004**, *306*, 1002–1005. [CrossRef] [PubMed]
17. Bellessa, J.; Bonnand, C.; Plenet, J.C.; Mugnier, J. Strong Coupling between Surface Plasmons and Excitons in an Organic Semiconductor. *Phys. Rev. Lett.* **2004**, *93*, 036404. [CrossRef]
18. Symonds, C.; Bonnand, C.; Plenet, J.C.; Bréhier, A.; Parashkov, R.; Lauret, J.S.; Deleporte, E.; Bellessa, J. Particularities of surface plasmon–exciton strong coupling with large Rabi splitting. *New J. Phys.* **2008**, *10*, 065017. [CrossRef]
19. Jacob, Z.; Shalaev, V.M. Plasmonics Goes Quantum. *Science* **2011**, *334*, 463–464. [CrossRef]
20. Pelton, M.; Storm, S.D.; Leng, H. Strong coupling of emitters to single plasmonic nanoparticles: Exciton-induced transparency and Rabi splitting. *Nanoscale* **2019**, *11*, 14540–14552. [CrossRef]
21. Moilanen, A.J.; Hakala, T.K.; Törmä, P. Active control of surface plasmon–emitter strong coupling. *ACS Photonics* **2018**, *5*, 54–64. [CrossRef]
22. Buzavaite-Verteliene, E.; Plikusiene, I.; Tolenis, T.; Valavicius, A.; Anulyte, J.; Ramanavicius, A.; Balevicius, Z. Hybrid Tamm-surface plasmon polariton mode for highly sensitive detection of protein interactions. *Opt. Express* **2020**. [CrossRef] [PubMed]
23. Azzini, S.; Lheureux, G.; Symonds, C.; Benoit, J.-M.; Senellart, P.; Lemaitre, A.; Greffet, J.-J.; Blanchard, C.; Sauvan, C.; Bellessa, J. Generation and Spatial Control of Hybrid Tamm Plasmon/Surface Plasmon Modes. *ACS Photonics* **2016**, *3*, 1776–1781. [CrossRef]
24. Arwin, H. TIRE and SPR-enhanced SE for adsorption processes. In *Ellipsometry of Functional Organic Surfaces and Films*; Hinrichs, K., Eichhorn, K.-J., Eds.; Springer: Berlin/Heidelberg, Germany, 2014; Volume 52, pp. 249–264, ISBN 978-3-642-40127-5.
25. Arwin, H.; Poksinski, M.; Johansen, K. Total internal reflection ellipsometry: Principles and applications. *Appl. Opt.* **2004**, *43*, 3028. [CrossRef] [PubMed]
26. Balevicius, Z.; Baleviciute, I.; Tumenas, S.; Tamosaitis, L.; Stirke, A.; Makaraviciute, A.; Ramanaviciene, A.; Ramanavicius, A. In situ study of ligand–receptor interaction by total internal reflection ellipsometry. *Thin Solid Film.* **2014**, *571*, 744–748. [CrossRef]
27. Balevicius, Z.; Talbot, J.; Tamosaitis, L.; Plikusiene, I.; Stirke, A.; Mickiene, G.; Balevicius, S.; Paulauskas, A.; Ramanavicius, A. Modelling of immunosensor response: The evaluation of binding kinetics between an immobilized receptor and structurally-different genetically engineered ligands. *Sens. Actuators B Chem.* **2019**, *297*, 126770. [CrossRef]
28. Paulauskas, A.; Tumenas, S.; Selskis, A.; Tolenis, T.; Valavicius, A.; Balevicius, Z. Hybrid Tamm-surface plasmon polaritons mode for detection of mercury adsorption on 1D photonic crystal/gold nanostructures by total internal reflection ellipsometry. *Opt. Express* **2018**, *26*, 30400. [CrossRef]
29. Buzavaite-Verteliene, E.; Valavicius, A.; Grineviciute, L.; Tolenis, T.; Lukose, R.; Niaura, G.; Balevicius, Z. Influence of the graphene layer on the strong coupling in the hybrid Tamm-plasmon polariton mode. *Opt. Express* **2020**, *28*, 10308. [CrossRef]